IMPLEMENTING LANIER'S PATENTS FOR STABLE, SAFE AND ECONOMICAL ULTRA-SHORT WING VACU- AND PARA-PLANES

Graeme C. Hocking*, Yvonne M. Stokes† and Winston L. Sweatman‡

Abstract

Six patents were secured by E.H. Lanier from 1930 to 1933 for aeroplane designs that were intended to be exceptionally stable. A feature of five of these was a flow-induced "vacuum chamber" that it was thought provided superior stability and increased lift compared to typical wing designs. Initially this chamber was in the fuselage, but later designs placed it in the wing by replacing a section of the upper skin of the wing with a series of angled slats. We investigated this wing design using inviscid aerodynamic theory and viscous numerical simulations and found no evidence to support the claims made. Rather we suggest that any improvement in lift and/or stability seen in the few prototypes that were built was due to thicker airfoils than was typical at the time.

1. Introduction

BackYard TEch are interested in aspects of aircraft design described by Edward H. Lanier in a series of six United States patents obtained from 1930 to 1933. Lanier's overall aim was to provide an exceptionally stable aeroplane that would both fly normally and recover from undesirable attitudes without pilot aid. BackYard TEch were specifically interested in Lanier's idea of creating a vacuum cavity in the wing by replacing a section of the upper skin of the wing with a series of

*Mathematics and Statistics, Murdoch University, Perth, WA, 6150, Australia. Email g.hocking@murdoch.edu.au
†School of Mathematical Sciences, University of Adelaide, South Australia, 5005, Australia. Email yvonne.stokes@adelaide.edu.au
‡Institute of Information and Mathematical Sciences, Massey University at Albany, Private Bag 102 904, North Shore Mail Centre, Auckland, New Zealand. Email w.sweatman@massey.ac.nz

angled slats, believing that this wing design would give superior lift and stability compared to typical wing designs.

The MISG group approached this problem with a background reading of Lanier's patents, calculations and study based on the basic theory of aerodynamics, numerical solution of potential flow around an ellipse, and numerical simulation of viscous flow around an airfoil. The effects of angle of attack, ground separation and wing thickness were considered. The complexity of the situation and lack of experimental data made mathematical modelling difficult. To the limited extent to which modelling was possible there was no indication that modern aeroplane design had overlooked a major feature which would improve flight characteristics. Lanier's designs from the 1930s are now over seventy years old and are perhaps more readily related to the pioneering aircraft of the early 1900's than to those of the present day.

Details obtained of aircraft studies based on Lanier's patents from the 1930's were very limited. A few non-technical articles appeared in contemporary popular science magazines. We were unable to find any reference or citation of the designs in the scientific literature. The main sources of information were Lanier's six US patents.

In this paper, we begin by briefly summarising flight theory and then attempting to put the designs of Lanier into some historical context. We then analyse the comments made by Lanier in the original patent documents. This is followed by some calculations made from the claimed performance of the vacu-plane in the existing documents, and calculations of lift made using an inviscid model. Next, results of viscous-flow simulations, done using the finite-element PDE solver *Fastflo* [3], for a 'slat-wing' (with open top surface) and a more conventional closed wing are compared. Finally, we look at viscous flow over a single slot, again using numerical simulations from the *Fastflo* PDE solver.

2. Background Theory and Historical Perspective

The theory of flight is now well-established. Aircraft undergo four different forces that dictate their flight characteristics: lift, weight, thrust and drag. In level flight, lift and gravitational forces are in balance. Similarly, at a constant speed, the forward thrust must be of the same magnitude as the drag created by the motion. The weight and thrust are characteristic of the aircraft with its load and the engine, respectively. Lift and drag are influenced by the aerodynamics of the plane's lifting surfaces and fuselage and, consequently, are the main fo-

cus of this work. More detailed discussions of what follows can be found in [1, 4].

Lift is usually recorded in terms of the lift coefficient C_L, which is a non-dimensional measure of lift that can be used in any consistent system of units. Thus the lift on an airfoil can always be calculated as $L = C_L \rho U^2 A/2$, where U is the speed, A = chord $\times$ span is the projected area of the lifting surface, and ρ is the air density. In a similar way, drag is recorded as a drag coefficient, i.e. C_D, where total drag is $D = C_D \rho U^2 A/2$.

Lift is generated by the difference in flow velocity above and below the wing. The air flows more quickly over the upper surface, and therefore has lower pressure (according to the Bernoulli equation) than the more slowly moving air under the wing. Factors influencing lift are the shape of the wing, the angle of attack and the proximity to the ground. Drag consists of two types, form and induced. Form drag is the effect of viscosity as the air "sticks" to the surface of the plane. Induced drag results from the fact that wings have a finite length; the flow of air around the wing tips, from the high pressure region below the wing to the low pressure region above it, creates trailing vortices that result in further drag.

Flight is a trade-off between lift and drag. Mechanisms that increase lift, such as additional flaps or small extra airfoils that prevent separation around the leading edge, usually have the effect of increasing drag. Modern aircraft usually have some of these additional devices that extend during take-off and landing where higher lift is desirable and extra drag is not so important (in fact during landing it is often desirable).

Lift is generally proportional to the angle α of the wing relative to the direction of travel or air flow (the angle of attack) and the square of the velocity. We assume that the wing span is long relative to its thickness and chord (breadth). Then the flow is essentially two-dimensional enabling us to consider flow in a plane containing a cross-section of the wing. Lift per unit wing-span can then be quantified by the formula $L = \rho U \Gamma$, where $\Gamma = \oint \mathbf{q} \cdot \mathbf{dr}$ around a loop containing the wing cross-section, is known as the circulation. (The circulation is not an actual flow.) This has to be determined subject to the Kutta condition; that the air flow separates smoothly from the (sharp) trailing edge of the wing. For relatively thin, symmetric wings, $\Gamma \approx \pi U \mathcal{C} \sin\alpha$, where $\mathcal{C}$ is the chord length of the wing, so that the lift per unit span is $L = \pi \rho U^2 \mathcal{C} \sin\alpha$, or $C_L = 2\pi \sin\alpha$.

However, if the angle of attack becomes too large, the flow no longer follows around the wing but separates from the upper surface leading to

a sudden and dramatic loss of lift called *stall*. The thicker the wing, the more likely this is to occur since the air has to divert more rapidly around the blunter leading edge, but it can also be influenced by the roughness of the surface, and in older aircraft, especially the early metallic bodies, this could play a significant role.

Aircraft from the time of the Wright Brothers until after World War I were mostly bi-planar. Biplanes typically had two thin wings made of wood and canvas held together by a variety of struts and wires. These were relatively light and so required less lift, but had high drag due to the wires, struts and rough surfaces.

Early monoplane wings were still quite thin, although they were fatter than biplane wings because the structural framework was internal. The slightly fatter wings generated slightly higher lift, but more powerful engines enabling higher speeds and hence considerably more lift (increasing with the square of speed) were a major factor in enabling the evolution of the monoplane. Rapid development between the two World wars led to planes designed for both long distance travel and high air speed, as adventurers tried to set records of both types. Further rapid advances in aircraft design during World War II, led to the first jet-powered craft.

3. Laniers Patents

Lanier registered six US patents for aeroplanes in the early 1930's namely 1750529 and 1779005 in 1930, 1803805 and 1813627 in 1931, 1866214 in 1932 and 1913809 in 1933 ([6]–[11]). Each patent is for an entire aircraft design and includes commentary on such matters as the windows and landing gear. The design aspect of interest here is the presence of cavities or slats on the upper surface of the wing and fuselage. In the early patents it was claimed that the cavity designs improved stability; later patents claimed enhanced lift as well. (The third of these patents [8] is not relevant here since it concerns an aeroplane with a top-wing and makes no reference to cavities or slats.)

Lanier in part attempted to explain increased lift from one or more cavities in the wings and/or fuselage as an effect of a partial vacuum set up in the aeroplane's wings and body. This space would then be at a lower density than the air surrounding the aircraft increasing buoyancy. Lanier also appears to anticipate an additional lift effect by exposing the inside top surface of the lower shell of the wing. Being patents the descriptions are on the whole general without detailed measurements. We now consider the patents in more detail.

The first two patents from 1930 introduce Lanier's idea of a "vacuum chamber". Essentially this is constructed by removing a portion of the upper wing surface allowing flow between the internal wing cavity

and the outside. At this stage there is no claim of additional lift from the design, the purpose of including the vacuum chamber being purely stability [6]:

> *" . . . it is an object to provide a machine that will not nose dive, side slip or tail spin under ordinary circumstances, but should this happen, the machine will right itself without the pilot aid."*

The second patent is directed towards larger machines and develops the idea of including a system of slats (or air buffers) across the hole in the upper wing surface. These buffers would not extend to the base of the vacuum chamber and would preferably be hinged so that they could close the top of the vacuum chamber when desired. Lanier argues for the inclusion of these buffers to reduce the flow of air into the vacuum chamber [7]:

> *"When the plane is moving at slow speed or the engine is throttled down, there is a tendency for the air to flow down into the vacuum chamber from above. The provision of the air buffers, however, causes this air to be deflected upwardly and rearwardly, thus preventing it from entering the vacuum chamber to any considerable extent."*

The buffers remained a feature of the later patents and with his fourth patent [9] Lanier made the further claim that his vacuum chamber increases lift in addition to improving stability:

> *" I have found by experiments and tests that the lifting power of the vacuum chamber exceeded my expectations, and I have further found that an aeroplane can be designed utilising the principle of the vacuum chamber lift in which the wings can be wholly eliminated or reduced to dwarf wings, . . . "*

The fifth patent [10] contains many of the earlier features and claims and is perhaps the most useful for obtaining an insight into Lanier's thoughts. He reiterates his goal of safety through stability but also mentions features that would be associated with a reduced wing size and increased lift. His vacuum chamber here extends to the whole of the wing and perhaps a portion of the fuselage and he explicitly claims that the partial evacuation of air leads to an increased lift. In addition to this lift, due to the buoyancy of a reduced air density within the plane (as in a balloon), Lanier also appears to claim a mechanical lift by exposing the bottom inner surface of the wing (in practice this would in part be offset by reduced lift on the inner top surface of the wing). He states that apart from the vacuum pocket the wings can be otherwise conventional:

> *"The theory of getting additional lift from a given wing area is applicable to the conventional wings of today with few changes, simply by making the wing air-tight and supplying vents or openings in the top surface to evacuate the air, thus increasing the payload without an increase in structural weight. Lift is also exerted on the inside bottom skin of the airfoil above the cabin which, on the conventional wing, is negligible. On planes with large cabins this additional lift would greatly increase payload."*

4. Lift Calculations

4.1. Simple calculations

In horizontal flight, the lift must balance the weight of the aircraft. Therefore, we can estimate the lift coefficient for the aircraft described in Lanier's patents by considering the weight.

Popular magazines indicate that the total mass of the Lanier XL-5 (1933) plane was not much more than M=220 kg including the pilot, and that they were able to take off at speeds as low as 48 km/hr ($\approx$ 13.3 m/s). At their cruising speed of $U = 128\,\mathrm{km/hr}$ ($\approx 35.6\,\mathrm{m/s}$) in level flight, the well known relation $L = C_L \rho U^2 A/2$, where A is the wing area (estimated at $A \approx 7\,\mathrm{m}^2$) and ρ is the density of air ($1.23\,\mathrm{kg/m}^3$ at 15°C and atmospheric pressure), gives an estimate for the lift coefficient of $C_L \approx 2Mg/(\rho U^2 A) \approx 0.40$, where $g = 9.8\,\mathrm{m/s}^2$ is the acceleration due to gravity. This is comparable with lift coefficients of conventional aircraft, both at that time and today.

The Lanier Paraplane Commuter 110 (see [2]) was built by Lanier aircraft corporation circa 1949, sixteen years after the original patents were submitted, and is of unknown design. This plane had similar takeoff and cruise speeds but a greater mass (640 kg), and roughly 30% greater wing area, giving a lift coefficient of $C_L \approx 0.88$, again within conventional values.

Further to this, we can estimate the drag coefficient by considering the maximum speed. The XL-5 had a 36 horsepower engine ($\approx 26\,\mathrm{kW}$), and an estimated top speed of 96 mph ($\approx 154\,\mathrm{km/h}$ or $43\,\mathrm{m/s}$). Drag $D = C_D \rho U^2 A/2$ and the power required is $P = D * U \approx 3.4 \times 10^5 C_D$ Watts, so $P \approx 340 C_D\,\mathrm{kW}$. The engine power is given as $P_E \approx 36\,\mathrm{Hp} \approx 27\,\mathrm{kW}$, so by comparing we see that the drag coefficient is $C_D \approx 0.079$.

The Lanier Paraplane Commuter 110 had a maximum speed of 165 mph or $\approx$ 74 m/s, but had a $150\,\mathrm{Hp} \approx 112\,\mathrm{kW}$ engine and slightly greater wing area; the same calculations give $P \approx 2300 C_D\,\mathrm{kW}$ and therefore a drag coefficient of $C_D \approx 0.049$.

In calculations to be described later, we have used an airfoil shape approximating the Clark-Y wing, see e.g. [4]. This choice was made for its visual similarity to the Lanier wing design (from sketches in the patents) for which the exact specifications are not known. Hence, for comparison, the lift and drag coefficients of this wing at 0° (6°) angle of attack are $C_L = 0.36\,(0.80)$ and $C_D = 0.0217\,(0.045)$.

These very simple calculations are based on information of slightly doubtful veracity, but indicate that there is nothing out of the ordinary in the behaviour of the Lanier aircraft.

A further implication in some of the popular literature and Lanier's patents (see above) was that there is a buoyancy effect of air being sucked out of the wing cavity. However, it is easy to show that the effect of reducing air density within the wings would have an almost negligible effect, perhaps lightening the aeroplane by a few hundred grams. For example, the total weight of air in a wing cavity with a volume of two cubic metres (estimated for the Lanier XL-4) is about 2.4 kilograms or around 1% of the total weight. However, since not all of the air could be evacuated, this is a very generous upper bound. In heavier, larger craft, this proportion would be greatly reduced.

In a stall situation, the pressure would equalise between the inside and outside of the wing, causing the air to rush back in, negating any buoyancy effect in free flight. It may be that the effect of drag on the lighter and slatted (and hence rougher) wings is greater than that on the engine and cabin, causing the plane to right itself as it falls, but this will depend on the plane's attitude at stall.

4.2. Inviscid Theory

In this section we compute the lift on an elliptic airfoil using an integral equation method so that we can compare the effects of wing thickness, angle of attack and the ground effect. The lift on an airfoil can be determined by inviscid flow theory. The assumption of irrotational flow of an inviscid, incompressible fluid in two-dimensions (assuming a large wing span) reduces the problem to that of solving for the velocity potential, Φ, where the velocity field $\mathbf{q} = \nabla\Phi$, and Φ must satisfy Laplace's equation $\nabla^2\Phi = 0$.

One way to do this is to compute the complex potential

$$w(z) = \Phi + i\Psi = Uz + \frac{i\Gamma}{2\pi}\ln(z^2 + H^2) + \chi(z),$$

where the first term represents the free stream flow with velocity U, the second the circulation around the wing, H is the height above the ground, and $\chi(z)$ is to be determined to satisfy the boundary conditions for the flow. Complex function theory says that the velocity potential Φ satisfies Laplace's equation provided $w(z)$ is an analytic function. Ψ is the streamfunction, and this must be constant on the surface of the wing, so that $\mathbf{q}\cdot\mathbf{n} = 0$, where $\mathbf{n}$ is the normal to the airfoil with upper and lower surfaces $y = f^{\pm}(x)$, i.e. there is no flow through the surface of the wing.

Using Cauchy's integral formula for the function $\chi(z) = \xi + i\eta$ around an integration contour including the body, an image body (symmetric

about the ground) and a circle of infinite limiting radius, leaves

$$\chi(z_0) = \frac{1}{2\pi i}\int_\gamma \frac{\chi(z)}{z - z_0}\, dz,$$

and γ consists of a path around the surface of the airfoil and its image beneath the line of symmetry of the ground. Defining an arclength s, where $ds = \sqrt{dx^2 + dy^2}$, and using the chain rule together with invoking the symmetry of the airfoil above the ground and its image, it can be shown that we obtain an integral equation for the real part of χ, i.e. ξ, as

$$\xi(s) = \frac{1}{\pi}\int_0^{s_L} \frac{\xi(t)[y'(t)\Delta x - x'(t)\Delta y] - \eta(t)[x'(t)\Delta x + y'(t)\Delta y]}{(\Delta x^2 + \Delta y^2)} \quad (1)$$

$$+\frac{\xi(t)[y'(t)\Delta x - x'(t)\Delta y_+] - \eta(t)[x'(t)\Delta x + y'(t)\Delta y_+]}{(\Delta x^2 + \Delta y_+^2)}dt, \quad (2)$$

where s_L is the arclength from the trailing edge of the body to the leading edge then back, and $\Delta x = x(t) - x(s)$, $\Delta y = y(t) - y(s)$ and $\Delta y_+ = y(t) + y(s)$.

Thus the method is to write the surface of the airfoil in parametric form $(x(s), y(s))$, and then take a discrete form of the integral using steps in arclength, $s_k, k = 1, 2, ..N$, and $\xi_k, k = 1, 2, ...N$. Replacing the integral by a sum, the unknown ξ_k can be obtained by solving N equations in N unknowns. This was all programmed using Fortran. Further details of the method can be found in [5].

We also know that the function $\chi(z) = \xi + i\eta$ is made up of the following components; $\xi(s) = \Phi(s) - Ux(s) + \frac{\Gamma}{2\pi}(\beta_1(s) - \beta_2(s))$ and $\eta(s) = \Psi_0 - Uy(s) - \frac{\Gamma}{2\pi}\ln\left[\frac{\rho_1(s)}{\rho_2(s)}\right]$ where Ψ_0 is the (constant) value of the stream function on the wing surface, $\beta_1 = \arctan(\frac{y-H}{x})$, $\beta_2 = \arctan(\frac{y+H}{x})$, $\rho_1 = (x^2 + (y - H)^2)^{1/2}$ and $\rho_2 = (x^2 + (y + H)^2)^{1/2}$ are the distances and angles to points on the surface. Thus, η is known everywhere on the surface and the integral equation can be used to find ξ and hence the velocity potential.

The crucial factor in determining the lift is the Kutta condition, which says that the flow detaches smoothly from the end of the airfoil. The circulation Γ must be chosen to ensure this condition is satisfied. This was achieved by allowing Γ to be one of the unknowns and including an extra equation to enforce this condition. In this case, since the trailing edge of an ellipse is blunt, it was enforced by ensuring the stagnation point formed on the trailing edge of the ellipse.

A series of simulations was performed using this code for various values of wing chord, thickness, angle of attack and height above the ground.

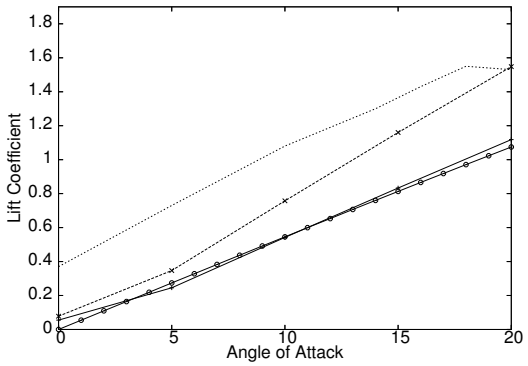

Figure 1. Lift (as lift coefficient C_L) on elliptic airfoils of maximum thickness 0.05 (+) and 0.3 (×) as angle of attack α varies, compared with the analytic formula for a flat plate (o). The approximate lift coefficients for a Clark-Y wing (which has thickness ≈ 0.12) are given as the upper line. Stall occurs at around 18.5°.

Figure 1 shows the results of increasing lift C_L with increasing angle of attack α and maximum thickness. These data are compared with the analytically computed formula for lift on a flat plate (or thin symmetric airfoil) and with the lift coefficient for the Clark-Y wing, which has maximum thickness of around 0.12. This non-symmetric airfoil is clearly much better designed than those used for numerical experiments. The stall of this wing at around 18° can be clearly seen (separation and stall are not computed as part of the other curves). The effect of wing thickness is seen in that for the elliptic airfoil the wing that is six times thicker has about 30% more lift at each angle of attack. Figure 1 illustrates that a "fatter" elliptic airfoil has a greater lift coefficient than a "thiner" airfoil.

Figure 2 shows the effect of proximity to the ground on the lift coefficient for several different thickness wings. It is clear that ground effect plays a role only when the ground is within one or two wing chord widths. These results suggest that we can neglect ground effect from our deliberations.

In general, wing profile designs must balance lift with drag. These results confirm that thicker wings tend to have higher lift for a given speed. However, they also tend to have increased drag making it more difficult to attain speed. In addition, thicker wings at higher speed are more likely to induce separation of the flow and hence stall (loss of lift).

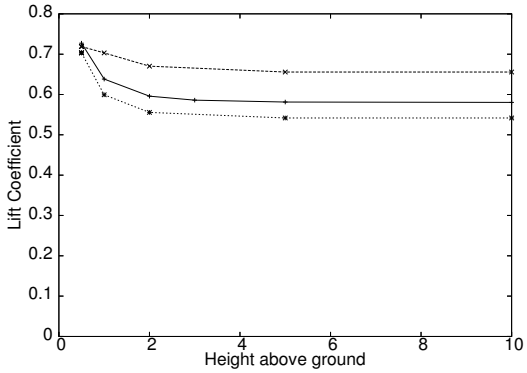

Figure 2. Lift (as lift coefficient C_L) on elliptic airfoils versus height above ground h (as a multiple of chord length) for thickness 0.05 ($*$), 0.1 ($+$) and 0.2 ($\times$), all at angle of attack of 10°.

At the time of Lanier's patents wings tended to be narrow in profile. However, one of his patents includes an illustration of a conventional wing together with the slatted wing of the patent design. The slatted wing is much fatter in profile than the conventional wing in the picture and if in practice this were the case then that could provide an explanation of increased lift for the Lanier aeroplane. The simple calculations in the previous section suggest that the lift of the Lanier craft was not exceptional compared to conventional airfoils such as the Clark-Y wing.

5. Numerical Simulations

5.1. Two-dimensional viscous flow over a wing

To compute the form drag of a wing, as well as its lift, we cannot use inviscid theory, but must solve for viscous flow around the airfoil. Hence, two-dimensional flow over thick and thin airfoils at different angles of attack has been simulated using the finite-element package *Fastflo* [3]. We here, necessarily neglect induced drag, which is a three-dimensional effect as described earlier, although it can be significant, especially for short wings. We have also made no attempt to compute form drag from the aircraft fuselage, focusing rather on the trade-off between lift and drag for a "slat-wing" compared to a conventional wing.

The geometries of the thick airfoils used in our simulations are shown in Figure 3. The basic airfoil shape superficially resembles the Clark-Y wing, see e.g. [4]. The chord length $\mathcal{C}$ of the airfoil is eleven times the

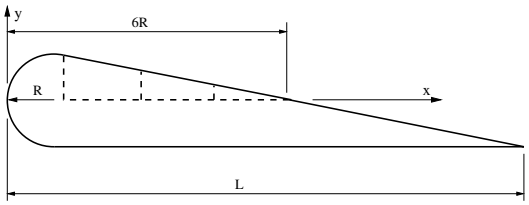

Figure 3. Typical 'thick' airfoil geometry. Conventional airfoil shown solid; cavity and vertical slats shown dashed.

nose radius R, which is the characteristic length for non-dimensionalisation. To complement flow over the conventional shape, the flow is also considered around a similar shape with a cut away cavity and slats to resemble the Lanier "slat-wing" design. The thin airfoil geometries are obtained by halving lengths in the vertical direction, giving a less blunt elliptical nose. Again a conventional closed airfoil and a "slat-wing" geometry are considered.

The flow is assumed to be two-dimensional, incompressible, steady and laminar, with a Reynolds number of 10. Although, Reynolds numbers of order 10^5 are to be expected, this is about the maximum that *Fastflo* can reliably handle for all simulations done, and no other simulation packages were available to the team during the MISG. We note also that the flow would almost certainly be turbulent, but only laminar flow has been considered due to constraints on time and facilities. Despite these draw-backs, the simulations still allow a comparison of the fundamental behaviour of a conventional wing and a Lanier "slat-wing". Separation of the flow from the airfoil is expected to occur at lower angles of attack for the blunt-nosed thick airfoil than for the thin airfoil.

We must solve the continuity and steady Navier-Stokes equations, subject to no-slip on the airfoil boundary, for the flow around four different airfoils (thick/thin $\times$ conventional/slat-wing). We adopt a reference frame that moves with the airfoil at speed U, and let x, y be the horizontal and vertical axes, respectively, with the origin at the tip of the nose of the airfoil (see Figure 3). Let u, v be the x, y components of velocity scaled with U, and let p denote pressure scaled with ρU^2. Lengths are scaled with the nose radius R. Then the dimensionless continuity equation is

$$\frac{\partial u}{\partial x} + \frac{\partial v}{\partial y} = 0 \tag{3}$$

and the Navier-Stokes equations are

$$u\frac{\partial u}{\partial x} + v\frac{\partial u}{\partial y} = -\frac{\partial p}{\partial x} + \frac{1}{R_e}\left(\frac{\partial^2 u}{\partial x^2} + \frac{\partial^2 u}{\partial y^2}\right), \tag{4}$$

$$u\frac{\partial v}{\partial x} + v\frac{\partial v}{\partial y} = -\frac{\partial p}{\partial y} + \frac{1}{R_e}\left(\frac{\partial^2 v}{\partial x^2} + \frac{\partial^2 v}{\partial y^2}\right), \tag{5}$$

where $R_e = UR/\nu$ is the Reynolds number, ν being the kinematic viscosity of air ($\approx 1.5 \times 10^{-5}\,\mathrm{m}^2/\mathrm{s}$). On the boundary of the airfoil we have $u = v = 0$. Far upstream of the airfoil, the flow is taken to be a uniform stream of magnitude U at angle of attack α. Sufficiently far above and below the airfoil we expect the flow to be that of a uniform stream also. Because we must solve over a finite computational domain, we define a square far field boundary having sides of length $20R$ around the airfoil, aligned with the flow and with centre at the tip of the nose of the airfoil $(x, y) = (0, 0)$. Thus, on the inlet (left), top and bottom boundaries we specify $u = \cos\alpha,\ v = \sin\alpha$. The outlet (right) boundary is a stress-free boundary. The far-field boundary is (hopefully) sufficiently far from the airfoil that the prescribed-velocity conditions do not impact too severely on the solution.

The finite-element PDE solver *Fastflo* was used to solve for the flow. *Fastflo's* automatic mesh generator was used to generate an unstructured mesh of about 1900 6-node triangles over the computational domain, with elements clustered more densely near the airfoil. The "augmented Lagrangian method" [3, §13.3] and quadratic basis functions were used to solve for pressure and velocity.

Having solved for velocity and pressure, lift and drag forces per unit wing-span are found by integrating the pressure around the surface of the airfoil $d\Omega$, i.e.

$$\frac{\mathbf{F}}{\rho U^2 R} = \oint_{d\Omega} p\, d\mathbf{r}.$$

and resolving the force per unit span $\mathbf{F} = (F_x, F_y)$ obtained into two components, one in the direction of the uniform stream (drag $D = F_x\cos\alpha - F_y\sin\alpha$) and the other normal to it (lift $L = F_x\sin\alpha + F_y\cos\alpha$). We may also find the lift and drag coefficients:

$$C_L = \frac{2L}{11\rho U^2 R}, \qquad C_D \approx \frac{2D}{11\rho U^2 R}.$$

These are given in Table 1 for different angles of attack for each of the simulations performed. Figures 4 and 5 show the lift and drag coefficients $C_L,\ C_D$ versus angle of attack α for each of the four airfoils considered.

Table 1. Lift and drag coefficients at angle of attack α for thick and thin conventional airfoils and slat-wings.

α		Conventional		Slat-wing	
		Thick	Thin	Thick	Thin
0	C_L	0.31	0.18	0.31	0.21
	C_D	0.21	0.11	0.24	0.13
5	C_L	0.54	0.54	0.53	0.55
	C_D	0.26	0.15	0.28	0.16
10	C_L	0.71	0.81	0.69	0.80
	C_D	0.33	0.23	0.35	0.23
15	C_L	0.83	1.04	0.82	1.05
	C_D	0.42	0.39	0.44	0.38
20	C_L	0.97	1.10	0.96	1.07
	C_D	0.54	0.46	0.55	0.45

Figure 6 shows the ratio of lift to drag coefficients, again versus angle of attack. In Figures 7–10 we show stream lines around the airfoils and velocity vectors near the upper surface behind the nose of the airfoils.

A comparison of the curve for the Clark-Y wing in Figure 1 with those for the thin wings in Figure 4 shows the lift coefficients to be of a similar order of magnitude at the same angle of attack and gives some assurance that the general behaviour of the wings under investigation is captured by our low Reynolds number simulations. It is expected that at higher Reynolds numbers boundary layers will be thinner and lift coefficients a little larger. In keeping with known aerodynamic behaviour, the lift coefficient for the thick wings is larger than for the thin wings at small angle of attack, however the slope of the curve C_L versus angle of attack α is greater for thin wings than for thick wings so that this situation reverses at larger angle of attack. (For thin symmetric wings $C_L/\sin\alpha \sim 2\pi$, while we have $C_L/\sin\alpha \sim 4$ for the thin asymmetric airfoils considered here.) For the thin wings, there is a sudden decrease in slope above $\alpha = 15^\circ$ signaling imminent stall (loss of lift). This is due to flow separation which occurs at about $\alpha = 15^\circ$ as seen in the plots of streamlines and velocity vectors given in Figures 9–10. The thicker wings experience flow separation at a lower angle of attack $\alpha \sim 10^\circ$, as seen in Figures 7–8, but do not exhibit such a sudden reduction in lift. It is readily seen that the conventional airfoil and corresponding slat-wing, whether thick or thin, differ little from one another in terms of lift coefficient.

As is to be expected the drag coefficient increases with angle of attack as seen for all airfoils in Figure 5. For the thin airfoils we have $C_D \approx$

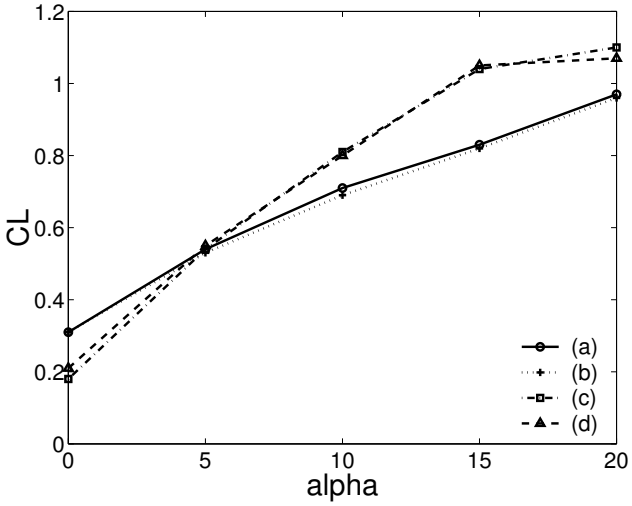

Figure 4. Lift coefficient C_L versus angle of attack α. (a) Thick conventional wing, (b) thick slat-wing, (c) thin conventional wing, (d) thin slat-wing.

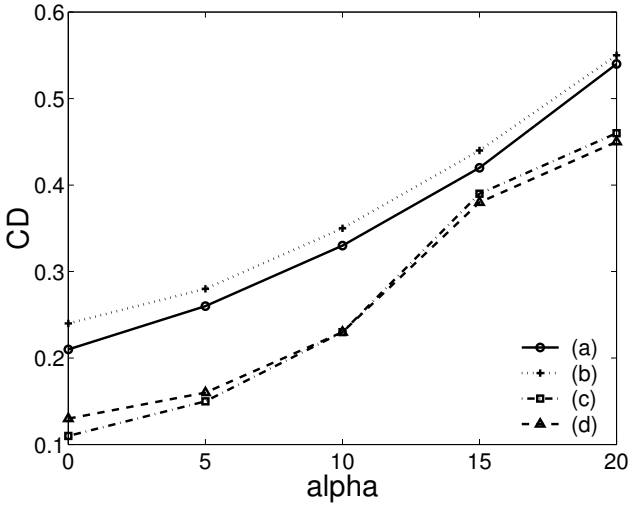

Figure 5. Drag coefficient C_D versus angle of attack α. (a) Thick conventional wing, (b) thick slat-wing, (c) thin conventional wing, (d) thin slat-wing. Reynolds number used is 10.

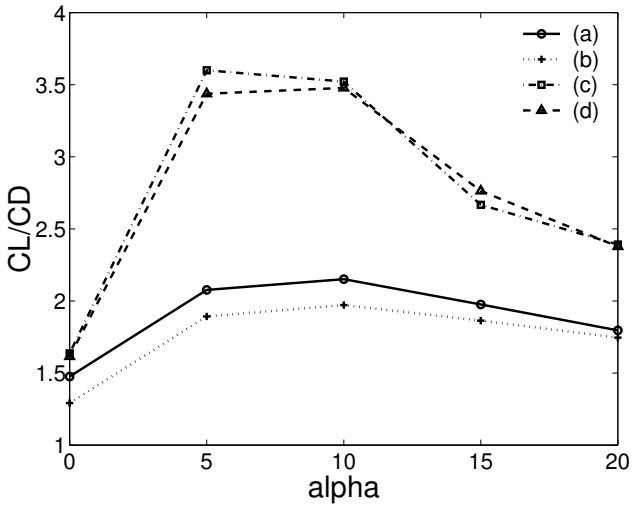

Figure 6. Ratio of lift to drag C_L/C_D versus angle of attack α. (a) Thick conventional wing, (b) thick slat-wing, (c) thin conventional wing, (d) thin slat-wing. Reynolds number used is 10.

$0.1\,(0.15)$ at $\alpha = 0^\circ\,(5^\circ)$ compared with $C_D \approx 0.022\,(0.045)$ for the Clark-Y wing. It is expected that, with thinner boundary layers at higher Reynolds numbers, drag coefficients will be lower than indicated by our simulations. From $\alpha = 10^\circ$ to 15° there is a significant increase in drag for the thin wings, which may be attributable to a relatively large increase in the projection of the surface area normal to the flow, an effect which would be smaller for thicker airfoils. There appears to be a slight increase in drag for the thick slat-wing compared to the thick conventional wing, but there is little difference in the C_D versus α curves between the thin conventional wing and the thin slat-wing.

The curve of lift to drag ratio C_L/C_D versus angle of attack (Figure 6) indicates that the thick and thin airfoils are most efficient over the range $\alpha = 5 - 10^\circ$. For the thick airfoils it is evident that the conventional shape is superior to the slat-wing in giving slightly more lift, less drag and, consequently, a higher lift to drag ratio at a fixed angle of attack, over the full range of angles considered. For the thinner wings, the conventional and slat-wing profiles are very similar excepting at $\alpha = 10^\circ$ where the conventional wing again appears to be superior.

Although we are mindful of the fact that our computations are not very accurate, the clear message emerging from our work is that our simulations certainly provide no evidence to support the slat-wing over conventional airfoils, but, if anything, the reverse.

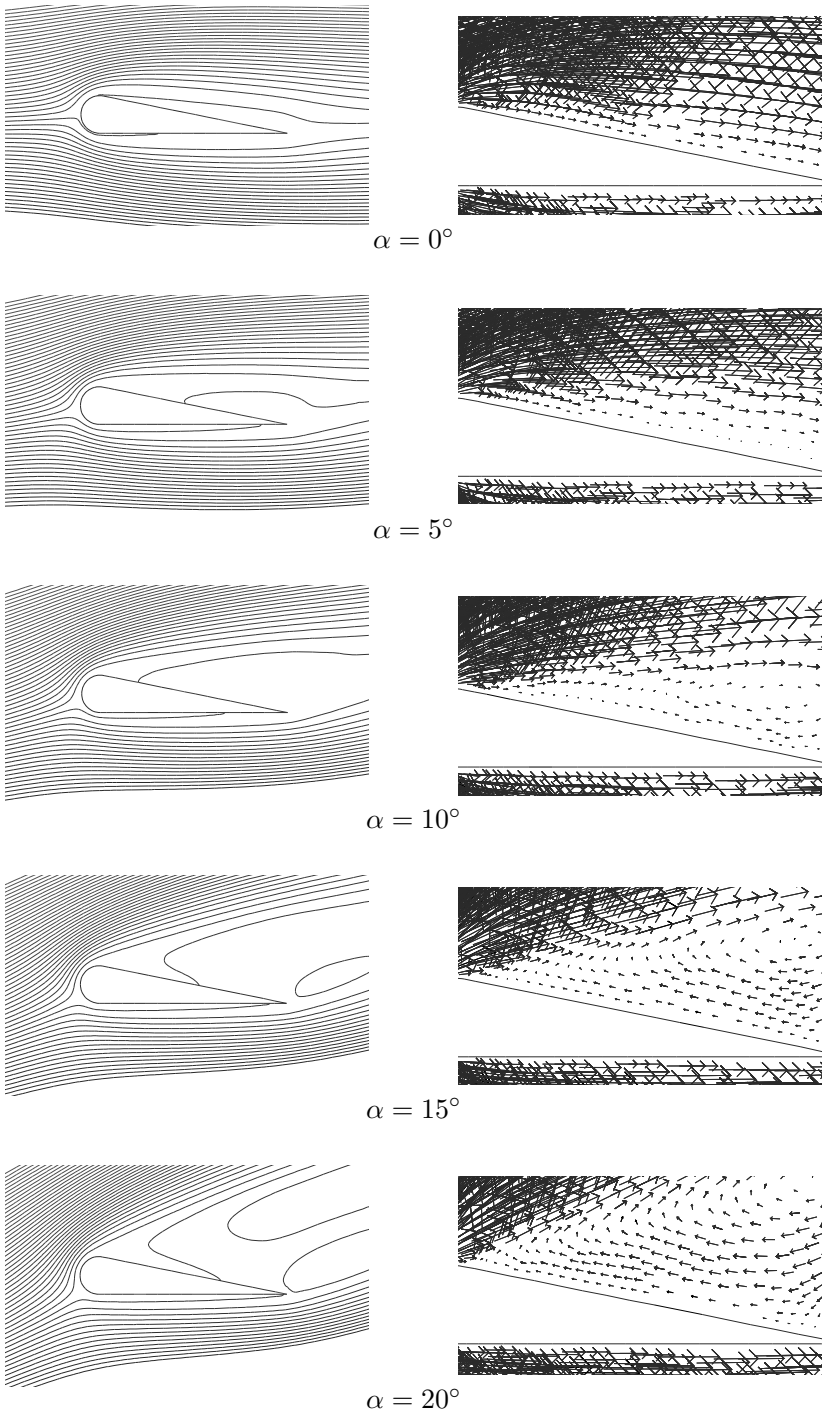

Figure 7. Thick, conventional airfoil. Streamlines and velocity vectors.

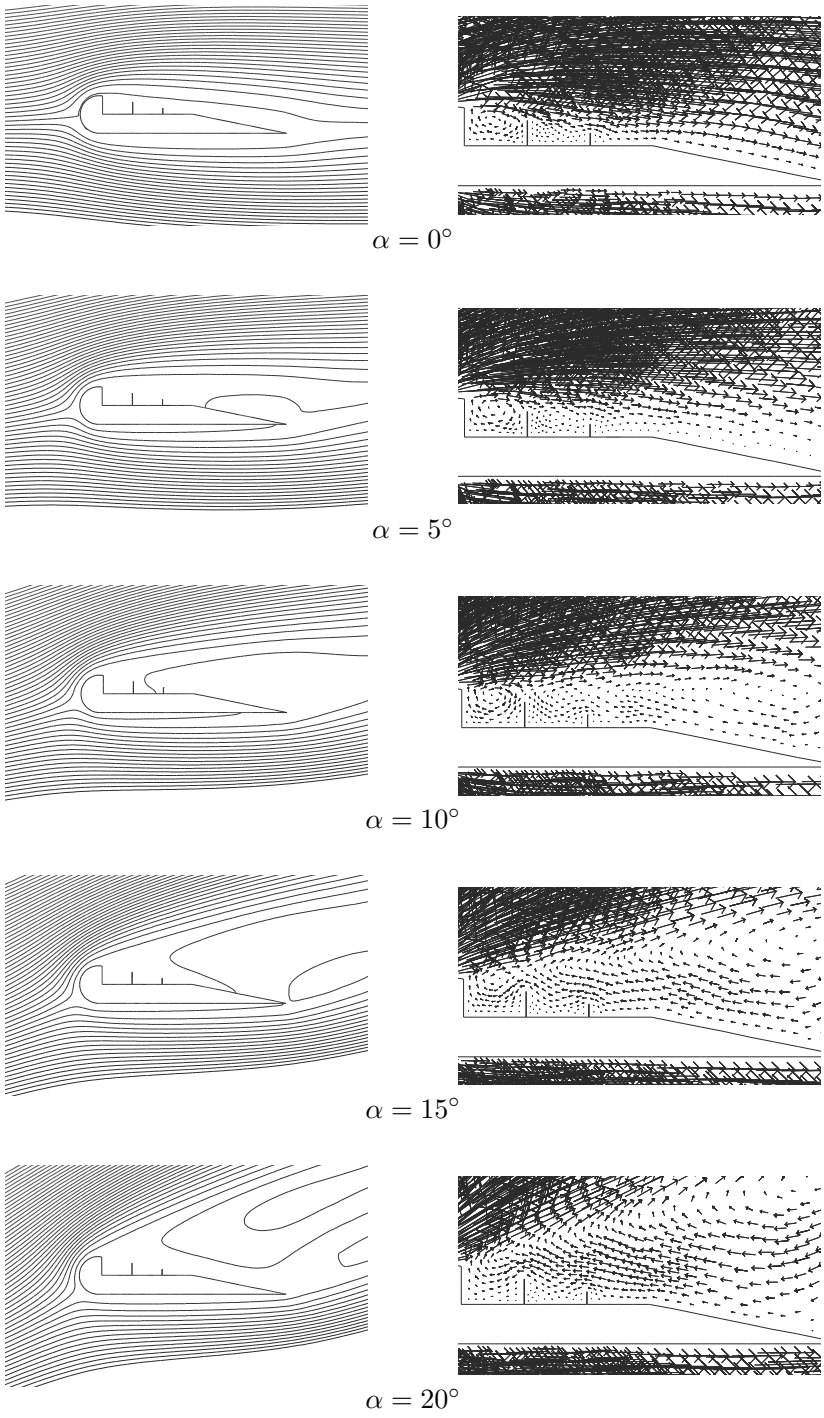

Figure 8. Thick, "slat-wing" airfoil. Streamlines and velocity vectors.

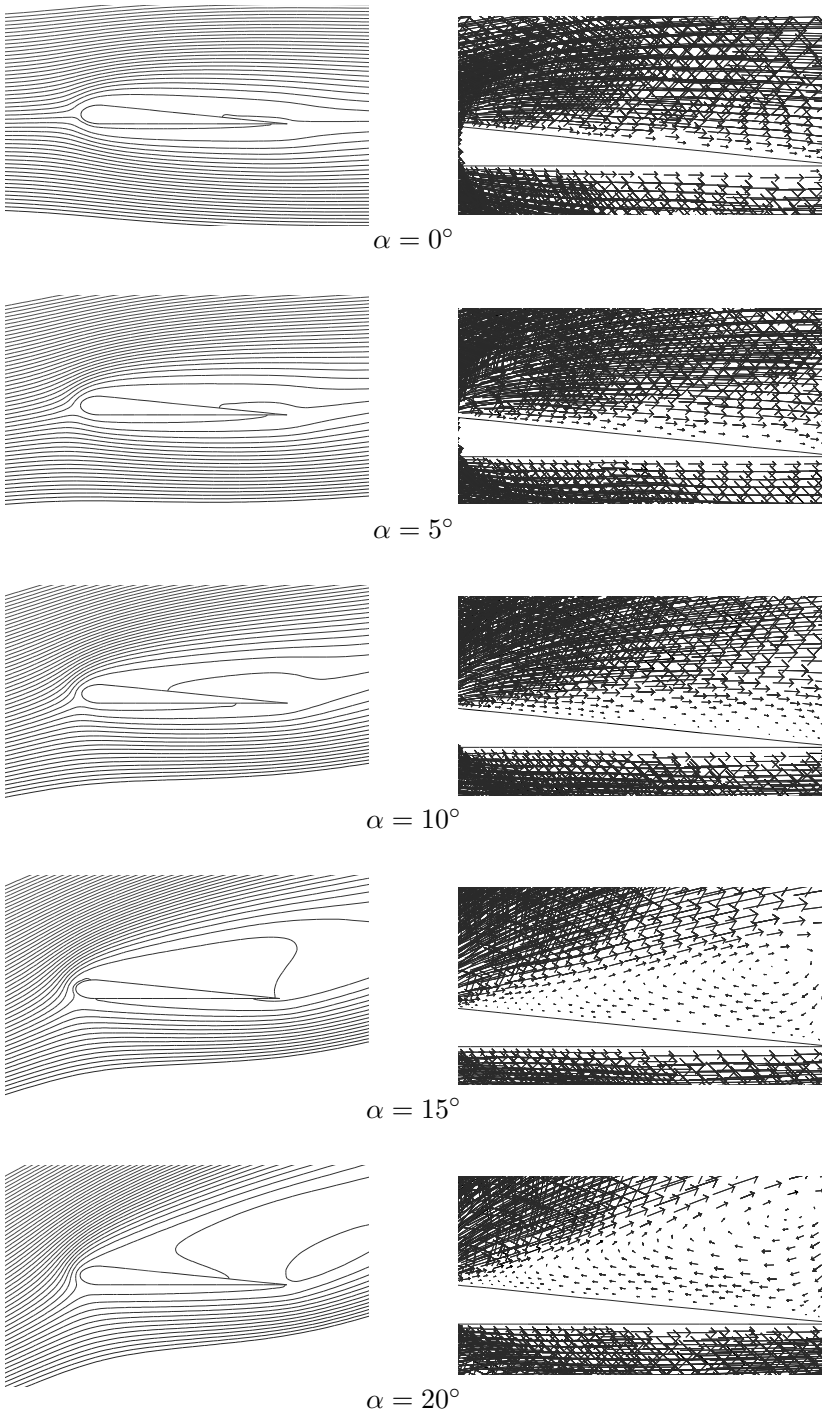

Figure 9. Thin, conventional airfoil. Streamlines and velocity vectors.

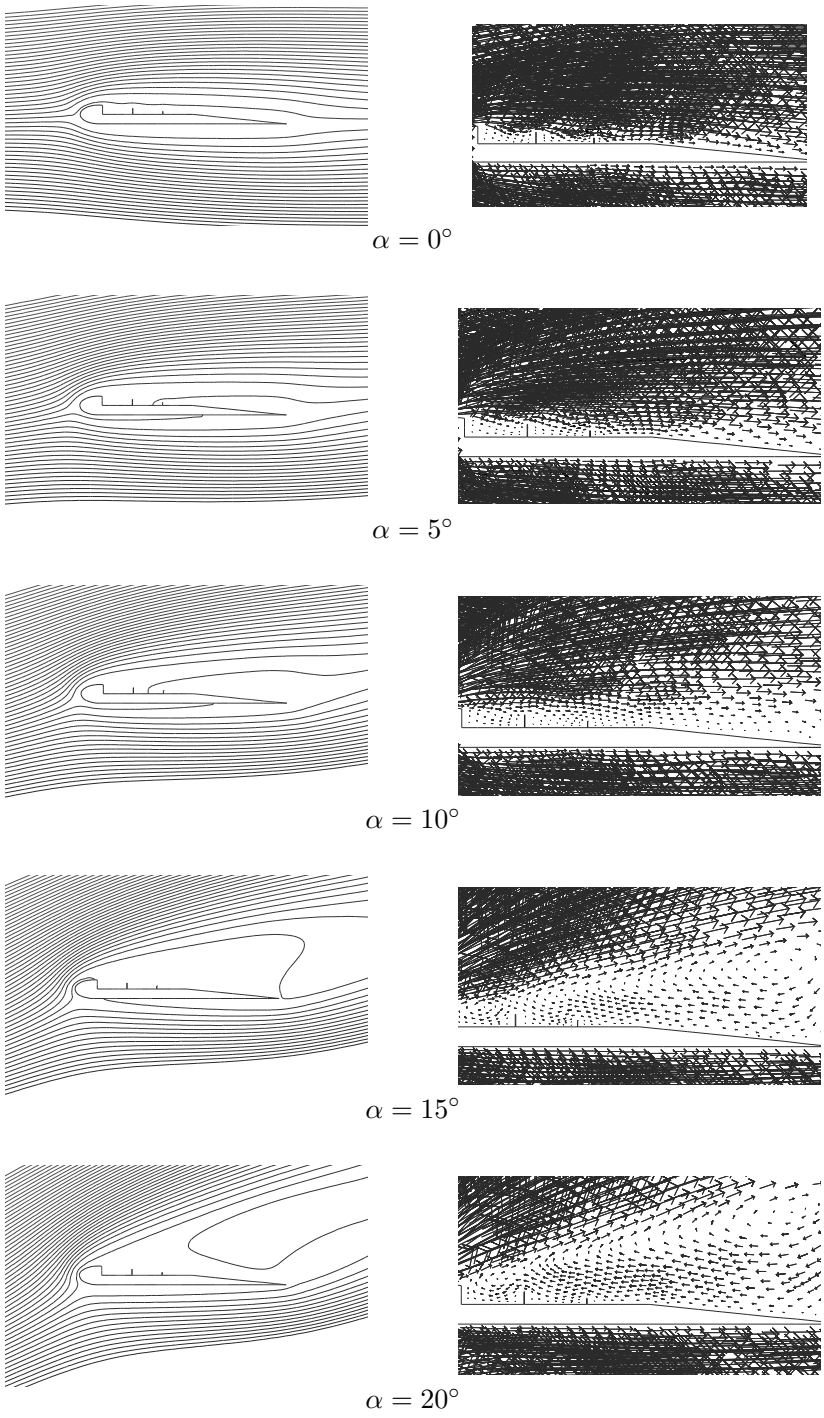

Figure 10. Thin, "slat-wing" airfoil. Streamlines and velocity vectors.

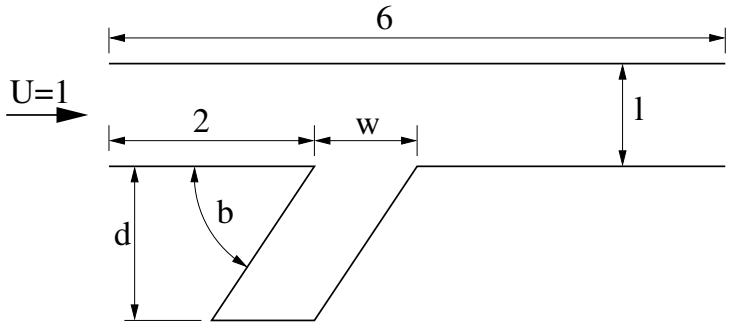

Figure 11. Geometry used for simulations of flow over a slot cavity. Slot aspect ratio is defined as $\varrho = w/d$

5.2. Modelling flow over a slot

Some further numerical simulations were conducted to illustrate the general features of flow over a slot cavity. The typical dimensionless geometry used in simulations is shown in Figure 11. The continuity and Navier-Stokes equations (3)–(5) were solved, again using *Fastflo* and the augmented Lagrangian method with quadratic basis functions. At the inlet (left boundary) we specified the flow to be that of a unit uniform stream ($U = 1$), while the outlet (right) was defined to be a stress-free boundary. The lower boundary containing the cavity is, of course, a no-slip boundary ($u = v = 0$); at the upper boundary we specified no normal flow ($v = 0$) and no tangential stress, i.e. this is a slip boundary. A mesh of about 3000 6-node triangles was used over the computational domain.

The effect of slot aspect ratio ($\varrho = w/d$) and slot angle β were considered to a limited extent. Pressure contours and streamlines are shown in Figure 12 for a cavity of depth $d = 1.5$ and width $w = 1$ at angles of inclination $\beta = 60°, 90°, 120°$. These were computed at a Reynolds number of $R_e = 1000$; at higher Reynolds numbers convergence difficulties were experienced. The results shown are typical of cavities of both larger and smaller aspect ratio, although the width and depth of the slot does vary the vortex flow and pressure. As can be seen, a vortex develops in the slot. The pressure at the centre of this vortex is lower than the average pressure in the surrounding fluid, but the overall pressure in the slot is very similar to that in the fluid immediately above the slot. This confirms our earlier findings that slots in the upper surface of the wing make little difference to the lifting capacity of the wing.

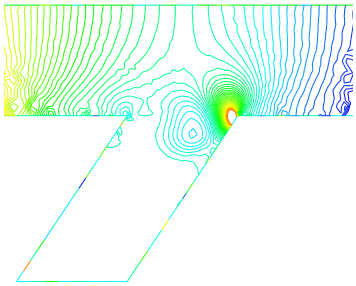

Pressure, $\beta = 60°$.

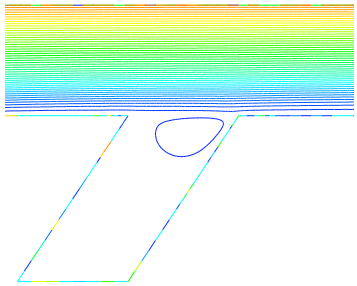

Streamlines, $\beta = 60°$.

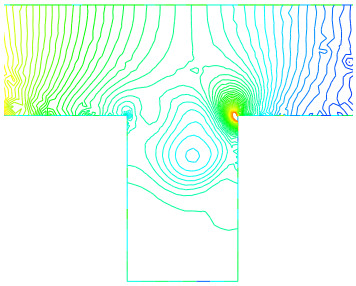

Pressure, $\beta = 90°$.

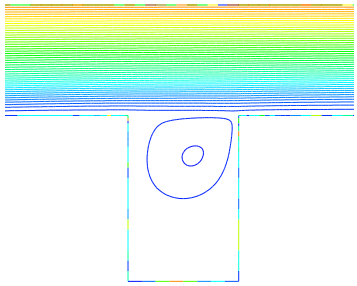

Streamlines, $\beta = 90°$.

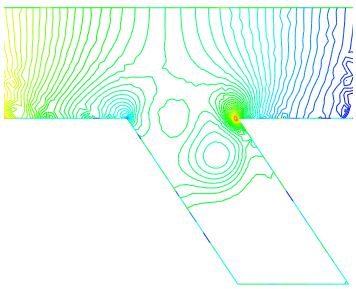

Pressure, $\beta = 120°$.

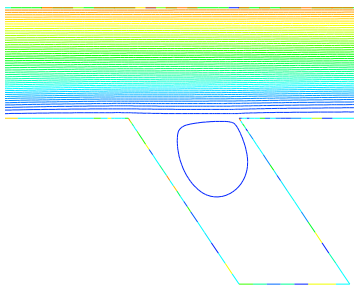

Streamlines, $\beta = 120°$.

Figure 12. Flow in the vicinity of a slot of aspect ratio $\varrho = 3/2$ ($d = 1.5,\ w = 1$) at various angles of inclination β. The colour of contours from blue to red indicates the change in value from lowest to highest.

6. Conclusions

The MISG team investigated the Lanier slat-wing design to determine whether there is any scientific basis to the claims, made in the patents, of superior stability and lift compared with conventional airfoils. We, necessarily, focused on lift and drag, as an investigation of stability required resources beyond those available to us. Our preliminary computations indicate that conventional airfoils are superior, or at least equivalent, to the Lanier slat-wing in terms of lift at a Reynolds number of 10. We suggest that the apparent improvement in lift and/or stability reported in the popular science literature of the times after experiments with one or two prototypes, was a result of using thicker airfoils than was typical at the time, so as to accommodate a "vacuum chamber" in the wing. As shown above (see e.g. Figure 1), thicker airfoils generate more lift at small angles of attack compared with thin airfoils. Possibly they also appeared to be more stable to Lanier and co-workers, since they would not undergo such a sudden stall as a thin wing. The rougher top surface due to the slats would almost certainly lead to separation at lower speeds and hence prohibit their use at higher speeds. It seems likely that *even if* the slat wing design provided some improvement on its contemporaries, it has now been superseded by modern wing designs that include variable wing shapes, auxiliary lifting surfaces and flaps that provide greatly enhanced performance, especially during take-off and landing.

The investigation of Lanier's designs could be extended. Probably the most natural approach would be to compare airfoils using wind tunnel experiments. Improved numerical experiments at higher Reynold's number might also help illuminate the problem. Further historical research might find out more from the 1930's to add to the largely anecdotal information available. The possible stability features at low speed appear the most promising aspect. It could be interesting to see how the Lanier design compared with contemporary aircraft of the 1930's. However, it appears unlikely that any such study would have an impact on modern aircraft design.

Acknowledgments

The moderators Graeme Hocking, Yvonne Stokes and Winston Sweatman thank all those who participated in this project: Syed Naeemul Ahsan, John Cogill, Bernard Ee, Ian Howells, Sam Howison, David Jenkins, Robert McKibbin, Tom Montague, Henning Rasmussen, Tony Roberts, Alfred Sneyd, Shixiao Wang and Pat Howden from Backyard Technology who brought the problem to MISG. YS also thanks Ernie Tuck for some useful discussion.

References

[1] Acheson, D.J., *Elementary fluid dynamics*, Clarendon Press, Oxford, UK, 1990.

[2] Bowers, P.M, *Unconventional Aircraft*, TAB Books, Blue Ridge Summit, PA, 1984.

[3] CSIRO, *Fastflo version 3, Tutorial Guide*. Commonwealth Scientific and Industrial Research Organisation (CSIRO), Australia, 1999.

[4] Jones, B., *Elements of practical aerodynamics*, New York: Wiley and Sons, 1950.

[5] Scott, B., "A boundary integral method for the solution of ground effect problems", Honours Dissertation, Dept. of Mathematics, University of Western Australia, 1994.

[6] United States Patent Office, Patent 1750529, March 11, 1930, Edward H. Lanier, of Miami, Florida. Aeroplane.

[7] United States Patent Office, Patent 1779005, October 21, 1930, Edward H. Lanier, of Miami, Florida. Aeroplane.

[8] United States Patent Office, Patent 1803805, May 5, 1931, Edward H. Lanier, of Miami, Florida. Aeroplane.

[9] United States Patent Office, Patent 1813627, July 7, 1931, Edward H. Lanier, of Miami, Florida. Aeroplane.

[10] United States Patent Office, Patent 1866214, July 5, 1932, Edward H. Lanier, of Miami, Florida. Aeroplane.

[11] United States Patent Office, Patent 1913809, June 13, 1933, Edward H. Lanier, of Covington, Kentucky. Aeroplane.